6-16-2015

# Ground-Penetrating Radar Velocity Determination and Precision Estimates Using Common-Mid-Point (CMP) Collection with Hand-Picking, Semblance Analysis, and Cross-Correlation Analysis: a Case Study and Tutorial for Archaeologists

Robert W. Jacob
*Bucknell University*, rwj003@bucknell.edu

T.M. Urban
*Cornell University*

# *Ground-penetrating radar velocity determination and precision estimates using common-mid-point (CMP) collection with hand-picking, semblance analysis, and cross-correlation analysis: A case study and tutorial for archaeologists*

R. W. Jacob[1]* and T. M. Urban[2]

1. Bucknell University 2. Cornell University, formerly Oxford University

*Accepted for publication 16 June 2015 in Archaeometry (University of Oxford) published by Wiley*

Abstract:

The most crucial parameter to be determined in an archaeological ground-penetrating radar (GPR) survey is the velocity of the subsurface material. Precision velocity estimates comprise the basis for depth estimation, topographic correction, and migration, and can therefore be the difference between spurious interpretations and/or efficient GPR guided excavation with sound archaeological interpretation of GPR results. Here we examine options available for determining GPR velocity and for assessing the precision of velocity estimates from GPR data, using data collected at a small-scale iron working site in Rhode Island, United States. In the case study, initial velocity analysis of common-offset GPR profile data using the popular method of hyperbola fitting, produced some unexpectedly high subsurface signal velocity estimates, while analysis of common mid-point (CMP) GPR data yielded a more reasonable subsurface signal velocity estimate. Several reflection analysis procedures for CMP data, including hand and automated signal picking using cross-correlation and semblance analysis, are used and discussed here in terms of efficiency of processing and yielded results. The case study demonstrates that CMP data may offer more accurate and precise velocity estimates than hyperbola fitting under certain field conditions, and that semblance analysis, though faster than hand-picking or cross-correlation, offers less precision.

*Keywords: Ground-penetrating radar (GPR), common-mid-point (CMP) analysis, semblance analysis, velocity migration*

* Corresponding Author: Robert W. Jacob, Ph.D., Assistant Professor.
Department of Geology, 231 O'leary Center, Bucknell University, Lewisburg, PA 17837
Office phone: +01(570) 577-1791. Fax: +01 (570) 577-3031
email address: rob.jacob@bucknell.edu

## 1.1 Introduction

Ground-penetrating radar (GPR) is commonly used in archeological investigations to provide three-dimensional imaging of subsurface features (e.g. Booth et al. 2008, Conyers 2013; Goodman and Piro 2013). The ability of GPR to rapidly and precisely estimate depths to features is the primary advantage of GPR over other geophysical methods commonly used in archaeology, especially given that accurate and precise subsurface spatial control is crucial to most archaeological work. The ability of GPR to accurately and precisely locate an archaeological object, feature, or strata is constrained by achievable resolution, which is in turn limited by the wavelength – in both the horizontal and vertical planes (Rial et al. 2007; Annan, 2009) and survey design – particularly in the horizontal plane (Urban et al. 2014 b; 2014 c). The wavelength is governed by antenna frequency and substrate velocity. When subsurface velocity is known, the wavelength in the medium can therefore be determined, and vertical resolution can be estimated as a fraction of the wavelength (Appendix A).

Knowledge of the subsurface velocity is also necessary for the implementation of several other GPR processing procedures which are important for successful archaeological investigations. Firstly, the accuracy and precision of depth estimates are dependent on knowledge of the subsurface velocity, for example Leckebusch (2007) shows that errors in velocity complicate depth determination. Secondly, topographic corrections, often undertaken for GPR surveys on uneven surfaces (e.g. Forte and Pipan, 2008), can be crucial in some instances to archaeological interpretation by mitigating any distortion within spatial correlations for reflected phases. Thirdly, the commonly used procedure of migration is often implemented to eliminate the tails of diffraction hyperbolas (e.g. Böniger and Tronicke, 2010). Successful migration generates GPR profile images which are more intuitive and have more appropriate dimensions for the embedded features which caused the diffraction hyperbolas. This latter procedure can be of great importance, particularly in archaeology, where interpretation of GPR (and other geophysical) data as cultural features is done largely on the basis of qualitative pattern recognition (Urban et al. 2014 a). While topographic correction and migration may be less crucial to archaeological interpretation than depth estimation, the procedures are of increasing importance as time-depth slicing and 3-D rendering has largely supplanted individual profile radargrams as the primary mode of presentation for archaeological GPR data (e.g. Doolittle and Bellantoni, 2010). The potential for false feature dimensions and other data artifacts from incorrect subsurface velocity can be more difficult to identify in 3-D rendering than in a profile by profile assessment. In either display mode, however, if hyperbolas are too numerous, the resulting interference pattern may make interpretation difficult without migration.

Knowledge of subsurface GPR signal velocity is therefore necessary for multiple reasons related to data processing; in addition, velocity estimates are crucial for guiding invasive subsurface investigations that may follow GPR work. This is not unknown in archaeologic studies (e.g. Pipan et al., 1999, Berard and Maillol, 2007, Quarto et al., 2007, Forte and Pipan, 2008, Böniger and Tronicke, 2010), but the precision of the velocity estimates is seldom assessed. While achievable resolution dictates the scale of objects and features that are identifiable by GPR and the minimum thickness necessary to identify an interface, the precision of depth estimates depends on precise traveltime observations. Factors such as GPR system characteristics, survey design, and analysis procedures affect the precision of traveltime observations. While a general statement of the precision associated with estimates of depth in archeological applications is provided by Conyers (2013), a method to determine the precision of such estimates is not provided nor is the related GPR signal velocity precision provided even though any knowledge of depth precision is hinged on this latter parameter. The uncertainty associated with the traveltime observations directly effects the precision associated with subsurface velocities and two-way travel time (TWTT) at zero-offset, and therefore limits the precision of depth estimation.

We summarize four common procedures to determine the subsurface GPR velocity and estimate of the precision, before offering a case study using GPR data from a historic iron smelting site is Rhode Island. The case study demonstrates the veracity of CMP data with semblance analysis in situations where other methods of velocity determination might fail. We show that identification of point scatterers in a GPR profile is often difficult and may lead to erroneous results. Further, we analyze CMP data to provide estimates for the precision of GPR signal velocity and TWTT to a reflection using two additional analysis methods. The three analysis methods differ in time required to produce the results. The separate precision estimates of TWTT and GPR signal velocity lead to the precision of the reflection depth. We compare the precision attained with different methods of GPR signal analysis for depths to subsurface reflectors and anthropogenic subsurface features.

## I.2 Methods of determining velocity

***Velocity tables:***

A commonly used method is to simply consult a table of known material velocity ranges (i.e. dry sand, wet sand, wet clay, limestone etc.) and select a likely velocity for the substrate at hand. For obvious reasons, this may result in an inaccurate velocity determination and therefore incorrect depth estimates, topographic corrections, and migration. Whenever possible, an empirical approach to velocity determination is therefore desirable.

***Implanted scatterer:***

A typical empirical method to estimate GPR signal velocity and thus depth is implanting a known object in the subsurface and collecting GPR data immediately above the object (Conyers, 2013). This method is difficult (often impossible) to employ at many archeological sites. In addition, the excavation process may produce error in the accuracy of the GPR signal velocity by altering hydrologic properties of subsurface (Conyers et al., 2002). The same will be true if a natural escarpment or previously open excavation is used (i.e. the soil will dry out, thus changing the velocity). A fresh excavation and compaction of excavated material to original porosity would therefore be required to ensure a reasonable estimate. This is however, contrary to the true benefits of GPR, which are the non-invasive nature of the method and the speed of data collection. Excavating and implanting a metal bar is simply stated, antithetical to these benefits. In addition, using only the travel time observation from directly above the metal bar leads to a GPR signal velocity estimate valid for only a very small lateral region of the site (total volume dictated by frequency of signal and electromagnetic properties of subsurface based on Fresnel Zone "illumination area"). Further, this approach does not allow for the estimation of signal velocity-precision which is independent of the depth-precision.

***Hyperbola fitting:***

GPR signal velocity may also be estimated from GPR profile data collected perpendicular to a subsurface "point scatterer" (Cross and Knoll, 1991; al Hagrey and Muller, 2000; Conyers, 2013). This method is based on the increasing traveltime associated with the increasing path length as distance increases away from the point scatterer. A hyperbola fitting method may be used (Stolte, 1994) and is typically employed in many GPR processing programs (e.g. Annan 2004). This method requires the presence of a point scatterer in the subsurface. Additionally, where velocity varies horizontally and vertically (as it frequently does), numerous (and clearly defined) scatterers may be required for an accurate estimate. While this situation sometimes presents itself at archaeological sites (e.g. Wolff and Urban 2013), in other situations, scatterers may be too infrequent or altogether absent thus rendering the method useless.

***Common mid-point (CMP)***

Collecting a CMP sounding is an alternate data collection method for GPR signals where the moveout (an increase in two-way traveltime) of a GPR phase (coherent signal on successive traces) increases with increasing path length due to increases in the offset between Transmitter (Tx) and Receiver (Rx) (see Appendix B for tutorial on CMP and see Annan (2004) for a more detailed

description). The observed moveout is used to solve for the velocity of the GPR signals and thus indicates whether the GPR signal is being reflected from an above ground or below ground target. Another benefit of CMP soundings is to provide the precision independently for both depth and GPR signal velocity estimates (Jacob and Hermance, 2004). The two-way traveltime data collected from a CMP sounding may be analyzed by picking the first break for the arrivals of direct, refracted and reflected phases and using either linear moveout analysis (Bohidar and Hermance, 2002) or normal moveout analysis (i.e. $T^2$-$X^2$ analysis, for example see Burger et al., 2006). However, picking the first breaks is time consuming if done by hand.

The GPR signal velocity may be efficiently determined from CMP sounding data using semblance analysis (Yilmaz, 2001), however, it is important to pre-analyze the data to eliminate direct and refracted phases from the analysis and to remove time base error (Jacob and Hermance, 2005). In addition, error in velocity measurements may be caused by uncertainty in antenna position, signal picking procedure, and a dipping interface relative to the ground surface (Barrett et al., 2007). The precision of GPR signal velocity and depth to reflecting interface from semblance analysis are independently estimated, however, the width of the resulting semblance peak will affect these estimates (Greaves et al., 1996). A limitation for CMP analysis is in areas with complex subsurface structure, where reflection analysis often fails to provide sufficient accuracy in GPR signal velocity (Yilmaz, 2001).

## 2. Case study methods

### 2.1 data collection

We collected GPR profile data using a sled setup deploying a PulseEKKO IV GPR system (Sensors and Software Inc) with bi-static 200 MHz unshielded GPR antennas and a single operator. The GPR antennas were one meter apart and oriented in broadside configuration. We then examined the profile upon completion and determined an appropriate location for a CMP sounding away from any point scatterers and other complexity in the subsurface. While a CMP may be collected in the presence of a point scatterer, we desired to have an independent estimate of velocity from the profile data (the latter of which used hyperbola fitting from point scatterers). The CMP sounding is completed by progressively increasing the separation (Tx-Rx offset) of the antennas in steps relative to the selected mid-point location along the original profile. Table 1 provides the specific GPR system parameters used for the data collection. The CMP data were also collected by a single operator using a sandbag to stabilize one antenna while the operator stabilized the other antenna.

### 2.2 Velocity estimation from CMP data

We assess three methods for estimating velocity from CMP data. GPR signal velocity may be determined by picking the first-break arrivals from the observed TWTT for specific direct, reflected, or refracted phases (Tillard and Dubois, 1995, van Overmeeren et al., 1997, Bohidar and Hermance, 2002). These picked arrivals are then analyzed using either linear moveout (LMO) analysis (the direct and refracted phases) or normal moveout (NMO) analysis (reflection phases). Trendlines are fit to the observed arrivals using a least mean square approach in either linear or squared space for LMO or NMO analysis, respectively. The precision of the GPR signal velocity estimate and TWTT at zero offset may then be estimated from the picked TWTT data by using a Student's T-Test at the 95% confidence limit (Jacob and Hermance, 2004). For either analysis method, the 95% confidence limit on the GPR signal velocity and traveltime may be estimated independently (Jacob and Hermance, 2004).

An alternate method to determine GPR signal velocity from the NMO of reflected phases in a CMP dataset is using semblance analysis (Yilmaz, 2001, Greaves et al., 1996). Semblance analysis provides a measure of signal coherency from one Tx-Rx offset to the next along a "hyperbolic trajectory governed by velocity, Tx-Rx offset, and TWTT" (Yilmaz, 2001). A velocity-TWTT spectrum is developed by calculating the signal coherency across all Tx-Rx offsets at the observed TWTT for a specified GPR signal velocity. This process can be automated using commercially available computer programs (e.g EKKO Project 2 by Sensors and

Software Inc.), and the resulting velocity spectrum may be contoured to reveal localized maximum coherence locations with a position in GPR signal velocity and TWTT at zero-offset for each reflection observed in the CMP data. Through this method a velocity structure of the subsurface above the deepest reflecting horizon is determined. The precision associated with this analysis may be estimated from the half-width of the maximum coherence (Greaves et al., 1996).

The final method we assess to determine GPR signal velocity is by cross-correlating each trace with the targeted GPR signal associated with the observed reflection. The first-break arrival of targeted GPR signal is the maximum correlation on each trace, thus instead of picking the first-break of the arrival for a GPR signal, the picking may be automated to locate the maximum (Hermance and Bohidar, 2002). These observations of first-break arrivals may then be analyzed using either LMO or NMO analysis. The 95% confidence limit precision of GPR signal velocity and TWTT at zero offset is estimated using the Student's T-Test (Jacob and Hermance, 2004).

## 3. Case study results

The raw GPR profile shows continuous reflections across the traverse from both flat lying and dipping interfaces, and several diffraction patterns indicative of point scatterers embedded in the subsurface (Figure 1a). The hyperbolic velocity analysis of five possible diffraction patterns (Figure 1b) interestingly exhibits variable tail spreads that would indicate lateral and vertical changes in the GPR signal velocities. The GPR signal velocity from the hyperbolic velocity analysis range between 0.07 m/ns and 0.136 m/ns over 8 m of profile distance (Table 2). These results may indicate there is a change in velocity with depth, where a shallow point scatterer (A) indicates a velocity of 0.11 m/ns while a deeper point scatterer (C) indicates a velocity of 0.080 m/ns. While rapid vertical changes in velocity may be true due to typical sedimentary, hydrologic, and anthropogenic layering, the interfaces will also produce strong reflections, which are not observed in the GPR profile (Figure 1). This wide range of GPR signal velocity over a short profile distance raises concern about the accuracy of any velocity estimate, but may also be indicative of the type of heterogeneity encountered in many archaeological settings (e.g. Leckebusch, 2007). Although, we observe that several of the diffraction patterns share traces with adjacent diffraction patterns, for example A and B on Figure 1b. In order for these velocities to be accurate, these point scatterers must therefore also lie outside of the proximate vertical plane of the GPR profile. However, a more likely possibility is that not all of the five diffraction patterns chosen for velocity analysis resulted from actual point scatterers, but rather that several are reflections from dipping interfaces that have generated diffraction-like patterns. The question then becomes which GPR signal velocity estimate to use for depth estimation, migration and topographic correction.

The CMP sounding data (Figure 2) collected at 7 m on the GPR profile, on the other hand, indicate at least two clearly identifiable reflected phases displaying NMO and the direct air phase displaying LMO. The first break picks on each trace – at each Tx-Rx offset – where these three phases were able to be identified are shown in Figure 2. The results of the LMO analysis for the direct air phase (Table 3) indicate that corrections to the time base of the GPR system were not necessary (Jacob and Hermance, 2005). The results of the NMO analysis of the first break picks from the deeper reflected phase and associated 95% confidence limit (Table 3) indicate the velocity to be 0.069 (±0.002) m/ns. The precision of the TWTT at zero-offset is ±0.5 ns. We minimized the possible sources of error in the velocity analysis during data collection and data analysis. However, the deep reflector dips eight degrees relative to the ground surface (Figure 1) which will cause error in the velocity determined from the CMP of one percent (Barrett et al., 2007) which is less than the estimated precision of the velocity analysis. The precision of the depth estimate combines the precisions associated with both TWTT and velocity, resulting in a confidence limit of ±10 cm from this analysis technique.

The results of the semblance analysis from the deeper reflected phase (Table 3) indicate a similar velocity to the first break picks. Although,

the time spent developing these estimates was one-third of the time spent developing the first-break estimates. The cost of this efficiency is in the TWTT precision, specifically the half-width in TWTT of the semblance maximum in Figure 3, which leads to a 95% confidence limit of ±30 cm for depth of the reflecting interface. In addition, the semblance analysis (Figure 3) illustrates that there is minimal vertical velocity variation at the location of the CMP sounding, unlike the hyperbolic analysis of point scatterers (Table 2).

The cross-correlation analysis involved constructing the native wavelet for the deeper reflection by removing NMO from 11 traces by shifting each trace (Figure 4). The corrected data were then stacked and averaged to construct the optimal stack (Figure 4a) which is then transformed into the native wavelet by making the initial deflection positive (Figure 4b). For each trace from the CMP sounding individually, the starting time ($\tau$) of the native wavelet is then increased and at each traveltime the cross-correlation product is calculated between the native wavelet and the GPR trace (Figure 4b). The result is a maximum negative correlation at the position of the first-break arrival of targeted GPR signal (Figure 4b). The traveltime for the maximum negative correlation value was automatically located on each trace. The result of the cross-correlation analysis from the deeper reflection (Table 3) indicates the best precision of all three methods, yielding a 95% confidence limit of ±5 cm for the depth estimate (less than the likely achievable vertical resolution). The total time required for this method was similar to that required for the first-break analysis, and two and three times longer than the semblance analysis.

The GPR profile data was corrected and interpreted based on the results of velocity analysis (Figure 5). In order to illustrate the concern of using the incorrect migration velocity, the shallow most velocity (0.11 m/ns) from diffraction analysis (Table 2) was used to migrate the GPR profile (Figure 5a). The GPR signal velocity from cross-correlation analysis of the CMP sounding data (0.071 m/ns) was also used to migrate the GPR profile (Figure 5b). The obvious difference in these two migration results is the depth, which becomes more significant with increasing depth. In addition, the most prominent change in these two images occur at depths less than 2 meters (<40 ns), where the migration velocity of 0.11 m/ns causes the shallow reflection to appear more continuous (Figure 5a compared to 5b). Interestingly, there are only subtle changes in how well either of these migration velocities collapsed the hyperbolic signatures from the diffractions. Although, image improvement is observed at positions <4 m and TWTT of 90 ns (Figure 5b compared to 5a).

The best estimate for substrate velocity (0.071 m/ns) attained using the CMP sounding was then used to topographically correct the GPR profile (Figure 5c). No hyperbolic signatures remain, indicating that the correct velocity was used for migration. There are two dominant layered reflections between 3.5 m and 15 m on the GPR profile, which agree with the shallow and deep reflections observed in the CMP sounding. The shallow reflection does not parallel the ground surface and is discontinuous. The deeper reflection is also discontinuous but is approximately horizontal and may be the watertable.

The migrated and topographically corrected GPR profile was interpreted (Figure 5d) and was used to guide subsurface excavation at the field site. The shallow reflection between 3.5 and 15 m was associated with layers of iron hardpan and slag produced during iron smelting operations. A deposit of several tuyeres, also associated with smelting operations, was located on the west end of the GPR profile centered at 2 m and at depths between 0.5 and 1.2 m. Excavation revealed the depth estimates provided from GPR survey were within the 95% confidence interval of the cross-correlation analysis.

**4. Discussion**

We have reviewed the advantages and disadvantage of some of the most popular methods of velocity determination and provided an empirical case-study where an implanted scatterer was unfeasible and hyperbola matching provided unreasonable results. While 3-D GPR data acquisition may have accounted for these

unreasonable results, provided they represented lateral changes in velocity, we desired a method to quickly collect data and determine depth to principal targets in order to better scope excavation work. We then evaluated three analysis procedures (hand-picking first breaks, semblance analysis, and cross-correlation) based on precisions associated with each and the time required for each to determine subsurface velocity from CMP data. Semblance analysis provided an efficient procedure to determine subsurface velocity and depth estimates, however, the precisions were significantly worse than either of the other more labor and time intensive procedures.

In order to place these precision estimates in context, we use the resolution of the GPR signal based on the Fresnel zone. The subsurface GPR velocity of 0.071 m/ns and the peak frequency of 120 MHz observed from the GPR data (determined from Hilbert analysis of the signal) mean that the wavelength was 0.6 m. In accordance with Annan (2004), the vertical resolution was 0.15 m for the observed GPR data (see Appendix A for details on resolution). The precision values in Table 3 for the depth estimates from first-break analysis and cross-correlation analysis were less than the calculated vertical resolution. Meanwhile, the precision for depth estimate (Table 3) from the semblance analysis exceeds the calculated vertical resolution. While the vertical resolution of the GPR signal provides the limitation for differentiating subsurface layers or targets, it does not limit the precision or accuracy of the observations. Thus, achieving precision estimates equal to or better than the vertical resolution of the GPR signal should be the goal of archaeological GPR studies.

## 5. Conclusions

Precision velocity estimates can be crucial for high quality archaeological GPR surveys. Many of the commonly used methods of velocity determination, however, may fall short in certain field conditions. We have described additional tools which have been less commonly used in archaeological geophysics for velocity estimation, and have further described an approach to assessing the precision of resulting estimates. While we are not endorsing CMP methods over other methods of velocity determination, we believe that this approach, which has seen limited use in archaeology, is worth adding to the archaeological geophysicist's tool-box. The approach may be especially useful for situations where sub-surface point scatterers are limited or unclear, thus resulting in biased or false depth estimates, in addition to inaccurate topographic corrections and migration.

**Acknowledgements:**

We thank John F. Hermance and Krysta Ryzewski respectively for use of the Brown University Environmental Geophysics facility and for access to the archaeological site used as the example in this paper. We also appreciate the suggestions and comments from L. Conyers and an anonymous reviewer, in order to improve this contribution.

## Appendix A. Vertical Resolution and GPR signals

The maximum achievable resolution in a GPR survey is largely a function wavelength $\lambda$, which is in turn determined by both velocity $V$ and antenna frequency $f$. This relationship can be described simply as,

$$\lambda = \frac{V}{f}$$

And this relationship may be altered to include the fundamental period or the pulse duration, $\tau_p$, (the inverse of frequency) of the GPR signal and related to vertical resolution, $\Delta_v$, as ¼ of $\lambda$ (Annan, 2004). And may be further related to the dielectric constant of the subsurface, $\varepsilon_r$, and the speed of light, $c$, assuming the magnetic permeability of free space.

$$\Delta_v \approx \frac{\tau_p V}{4} = \frac{\tau_p c}{4\sqrt{\varepsilon_r}}$$

The only parameter in these equations that we control is either $f$ or $\tau_p$. And by increasing $f$ (decreasing $\tau_p$) there will be a decrease in $\lambda$ and thus producing a smaller vertical resolution $\Delta_v$, referred to as a higher resolution. This is the principle reason that higher frequency antennas are used for archaeological GPR studies (Conyers, 2013) and non-destructive testing (NDT) studies (McCann and Forde, 2001), as well as other field studies where high resolution is a must. Alternately, in comparing different field sites, a decrease in $V$ will also result in a decrease in $\lambda$, and thus also producing a higher resolution. For this reason, lossy substrates often afford a higher resolution (Urban et al., 2014 b; Urban et al. 2014 c). While estimating vertical resolution as $\lambda/4$ is commonly used, it has been suggested, that with excellent data quality a vertical resolution as great as $\lambda/8$ could be possible under ideal conditions (Widess, 1973).

## Appendix B. CMP sounding tutorial

A CMP sounding is collected by increasing the Tx-Rx offset at a specific step size centered on the mid-point (Figure B1). The observed traveltime from each Tx-Rx offset position is then provided as an individual trace (Figure B2). The traveltime depends on the raypath that the GPR signal travels from the Tx to the Rx, specifically direct, refracted, or reflected. The two-way traveltime (TWTT) for the reflected raypath (Figure B1) has the following relationship between subsurface velocity, $V$, depth to the reflection interface, $D$, and Tx-Rx offset, $x$,

$$TWTT(x) = \sqrt{\left(\frac{x}{V}\right)^2 + \left(\frac{2D}{V}\right)^2}$$

Since the $x$ is measured carefully during data collection, the TWTT for the first break of the GPR reflected signal is only dependent on the two variables $V$ and $D$. In order to uniquely determine both variables, the TWTT for first-break of the reflected signal at more than one $x$ may be used to solve a system of equations (i.e. in Figure B2 solving the equation at $x = \alpha$ in terms of $V$ or $D$ and substituting into a second equation at larger $x$, where $x = \beta$). With more than two values of $x$, instead of solving a system of equations, the squared value of TWTT and squared value of $x$ for each first break pick from the reflected signal at all values of $x$ may be fitted with a linear trendline using a least-mean square approach (for example the trendline function in EXCEL). The slope of the trendline is equal to $\left(\frac{1}{V}\right)^2$ and the intercept of the trendline is equal to $\left(\frac{2D}{V}\right)^2$.

This equation of TWTT for a reflected signal is also the basis for semblance analysis described in the case study. Where the moveout for each GPR trace due to the increasing value of $x$ is removed from the observed TWTT based on a chosen value of $V$. If $V$ is correct, the reflected signal will arrive at a consistent value of corrected TWTT, and equal to $\left(\frac{2D}{V}\right)$. For further details on the CMP sounding method or semblance analysis the reader is referred to any of the following sources Annan (2005a), Annan (2005b), or Annan (2009).

**Sources:**

Al Hagrey and Müller, C., 2000. *GPR study of pore water content and salinity in sand*. Geophysical Prospecting, 48: 63–85.

Annan, J.P., 2004. *Ground Penetrating Radar: Principles, Procedures and Applications*. Sensors and Software Inc, Ontario.

Annan, A. P., 2005a. *GPR methods for hydrogeological studies* (pp. 185-213). In Hubbard and Rubin (Ed.), *Hydrogeophysics*. Springer Netherlands.

Annan, A. P., 2005b. *Chapter 11: Ground Penetrating Radar* (pp. 357–438), in: Dwain K. Butler (Ed.), *Near-surface Geophysics*, Investigations in Geophysics, vol. 13, Society of Exploration Geophysicists (2005)

Annan, A. P., 2009. *Chapter 1: Electromagnetic principles of ground penetrating radar* (pp. 3-40), in: Jol, H. M. (Ed.), *Ground penetrating radar theory and applications*, Elsevier (2009)

Barrett, B. E., Murray, T., & Clark, R., 2007. *Errors in radar CMP velocity estimates due to survey geometry, and their implication for ice water content estimation*. Journal of Environmental & Engineering Geophysics, 12(1), 101-111.

Berard, B. A., & Maillol, J. M., 2007. *Multi-offset ground penetrating radar data for improved imaging in areas of lateral complexity—application at a Native American site*. Journal of applied geophysics, 62(2), 167-177.

Bohidar, R. N., & Hermance, J. F., 2002. *The GPR refraction method*. Geophysics, 67(5): 1474-1485.

Böniger, U., & Tronicke, J., 2010. *Improving the interpretability of 3D GPR data using target–specific attributes: application to tomb detection*. Journal of Archaeological Science, 37(4), 672-679.

Booth, A.D., Linford, N.T., Clark, R.A., & Murray, T., 2008. *Three-dimensional, multi-offset ground-penetrating radar imaging of archaeological targets.* Archaeological Prospection, 15(2), 93–112.

Burger, H. R., Sheehan, A. F., & Jones, C. H., 2006. *Introduction to applied geophysics: Exploring the shallow subsurface*. WW Norton.

Conyers, L.B., Ernenwein, E.G., & Bedal, L. 2002. *Ground-Penetrating Radar Discovery at Petra, Jordan*. Antiquity, 76, 339-340.

Conyers, L.B., 2013. *Ground-Penetrating Radar for Archaeology*. Third edition. Altamira Press, Lanham, MD.

Cross, G. M., & Knoll, M. D., 1991. *Diffraction-based velocity estimates from optimum offset seismic data*. Geophysics, 56(12), 2070-2079.

Doolittle, J. A., & Bellantoni, N. F., 2010. *The search for graves with ground-penetrating radar in Connecticut*. Journal of Archaeological Science, 37(5), 941-949.

Forte, E., & Pipan, M., 2008. *Integrated seismic tomography and ground-penetrating radar (GPR) for the high-resolution study of burial mounds (tumul).* Journal of archaeological science, 35(9), 2614-2623.

Goodman, D., Piro, S., 2013. *GPR Remote Sensing in Archaeology*. Geotechnologies and the Environment, 9. New York: Springer Science.

Greaves, R. J., D. P. Lesmes, J. M. Lee, and M. N. Toksoz¨, 1996. Velocity variations and water content estimated from multi-offset, ground-penetrating radar. Geophysics 61: 683–695.

Hermance, J. F. & R. N. Bohidar, 2002. *Better Time Picks = Better Traveltimes = Better Velocities; Progress in Developing Public Domain Software*. Proceedings of the 9th Symposium on Ground penetrating Radar (GPR 2002), University of California, Santa Barbara (UCSB), April 29 - May 02, 2002.

Jacob, R. W., & Hermance, J. F., 2004. *Assessing the precision of GPR velocity and vertical two-way travel time estimates*. Journal of Environmental & Engineering Geophysics, 9(3), 143-153.

Jacob, R. W., & Hermance, J. F., 2005. *Random and non-random uncertainties in precision GPR measurements: Identifying and compensating for instrument drift*. Subsurface Sensing Technologies and Applications, 6(1), 59-71.

Jol, H.M.,(ed.), 2009. *Ground Penetrating Radar (GPR) Theory and Applications*. Elsevier Science, Amsterdam.

Leckebusch, J., 2007. Short Report: *Pull-up/pull-down corrections for ground-penetrating radar data.* Archaeological Prospection, 14(2), 142--145}

McCann, D.M. and M.C Forde, 2001. Review of NDT methods in the assessment of concrete and masonry structures, NDT & E International, Volume 34, Issue 2, Pages 71-84

Pipan, M., Baradello, L., Forte, E., Prizzon, A., & Finetti, I., 1999. 2-D and 3-D processing and interpretation of multi-fold ground penetrating radar data: a case history from an archaeological site. Journal of Applied Geophysics, 41(2), 271-292.

Quarto, R., Schiavone, D., & Diaferia, I., 2007. Ground penetrating radar survey of a prehistoric site in southern Italy. Journal of Archaeological Science, 34(12), 2071-2080.

Rial, F.I., M. Pereira, H. Lorenzo, P. Arias, A. Novo, 2007. Vertical and horizontal resolution of GPR bow-tie antennas. 2007 4th International workshop on *advanced ground penetrating radar.* IEEE proceedings.

Stolte, C., 1994. E-Migration: Image enhancement for subsurface objects of constant curvature in ground probing radar reflection data (Doctoral dissertation, Christian-Albrechts-Universität zu Kiel).

Tillard, S., and J. C. Dubois, 1995, Analysis of GPR data: wave propagation velocity determination. *Journal of Applied Geophysics* 33: 77– 91.

Urban, T.M., Clive Vella, Emanuela Bocancea, Christopher A. Tuttle, Susan E. Alcock. 2014 a. A geophysical investigation of a newly discovered Early Bronze Age Site near Petra, Jordan. *Journal of Archaeological Science* 42: 260 – 272.

Urban, T.M., Y.M. Rowan, M.M. Kersel. 2014 b. Ground-penetrating radar investigations at Marj Rabba, a Chalcolithic site in the lower Galilee of Israel. *Journal of Archaeological Science* 46: 96 -106.

Urban, T.M., J.F. Leon, S.W. Manning, K.D. Fisher. 2014 c. High resolution GPR mapping of Late Bronze Age architecture at Kalavasos-*Ayios Dhimitrios*, Cyprus. *Journal of Applied Geophysics*. Forthcoming.

Van Overmeeren, R. A., S. V. Sariowan, and J. C. Gehrels, 1997, Ground penetrating radar for determining volumetric soil water content; results of comparative measurements at two test sites. *Journal of Hydrology* 197: 316– 338.

Widess, M. B., 1973. How thin is this bed? *Geophysics* 38: 176-1180.

Wolff, C., T.M. Urban. 2013. Geophysical analysis at the Old Whaling site, Cape Krusenstern, Alaska, reveals the possible impact of permafrost loss on archaeological interpretation. *Polar Research* 32.

Yilmaz, Ö., 2001. Seismic data analysis (Vol. 1). Tulsa: Society of Exploration Geophysicists.

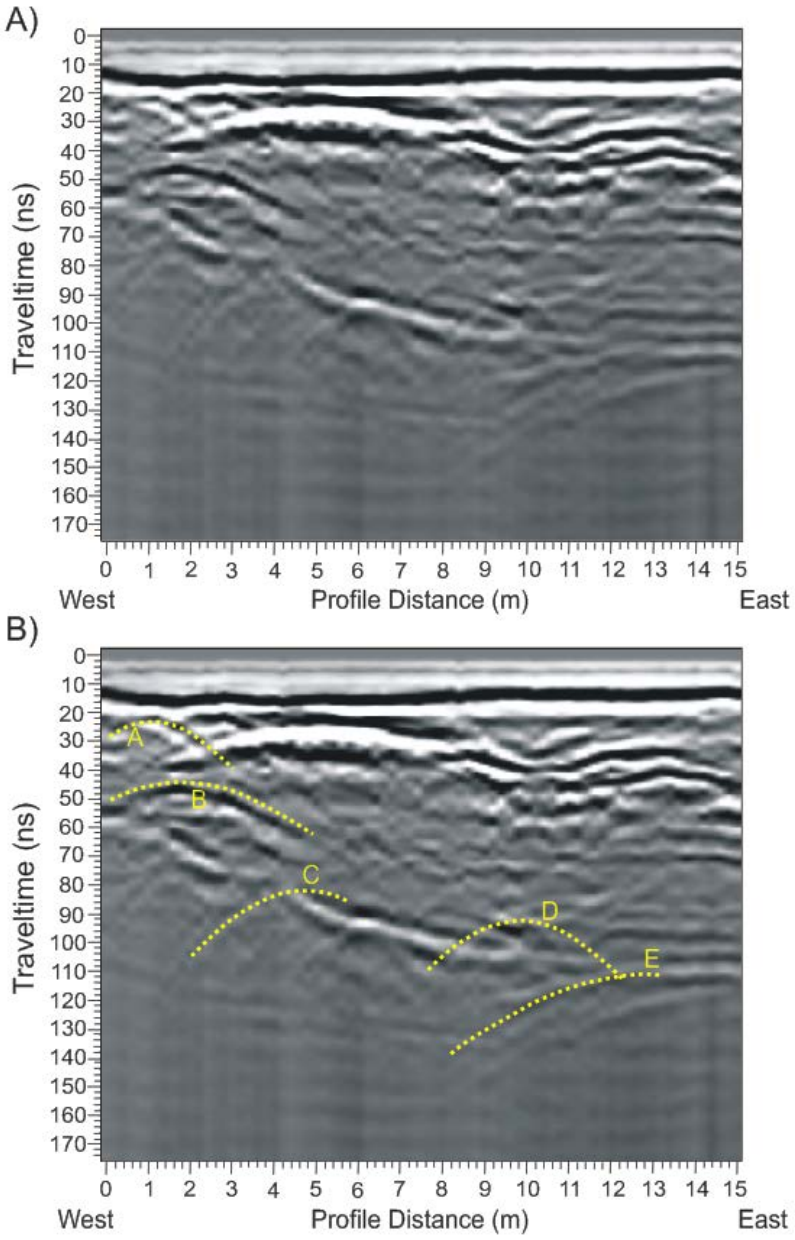


Figure 1. GPR profile data with Tx-Rx offset of 1 m in broadside configuration. A) GPR data with no processing showing both layered reflections and point scatterer reflections producing hyperbolic signatures. B) Raw data with observed hyperbolic signatures highlighted. Velocity analysis from each hyperbolic signature is provided in Table 2.

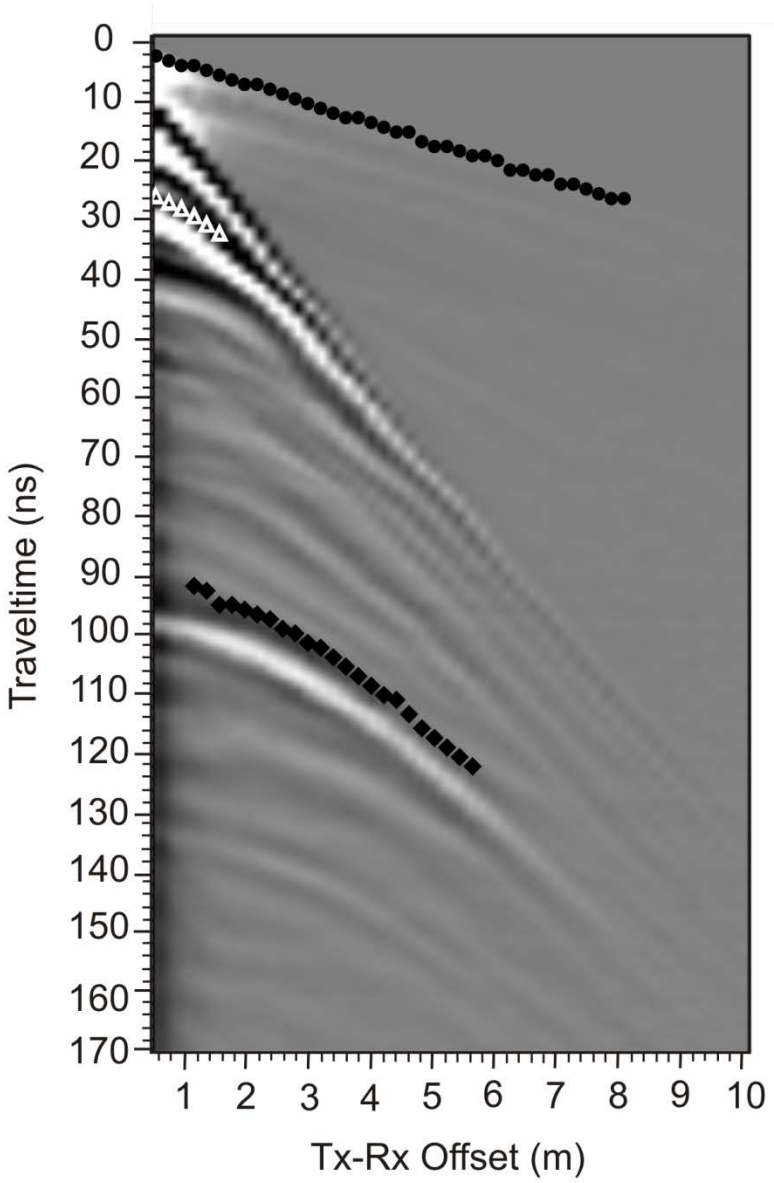


Figure 2. GPR CMP sounding data with no processing in broadside configuration collected at 7 m on the profile in Figure 1. Cross-correlation picks of the first arrivals for the direct air (black circles), shallow reflection (white triangles) and deep reflection (black diamonds) are provided. Velocity analysis from direct air and deep reflection are in Table 3.

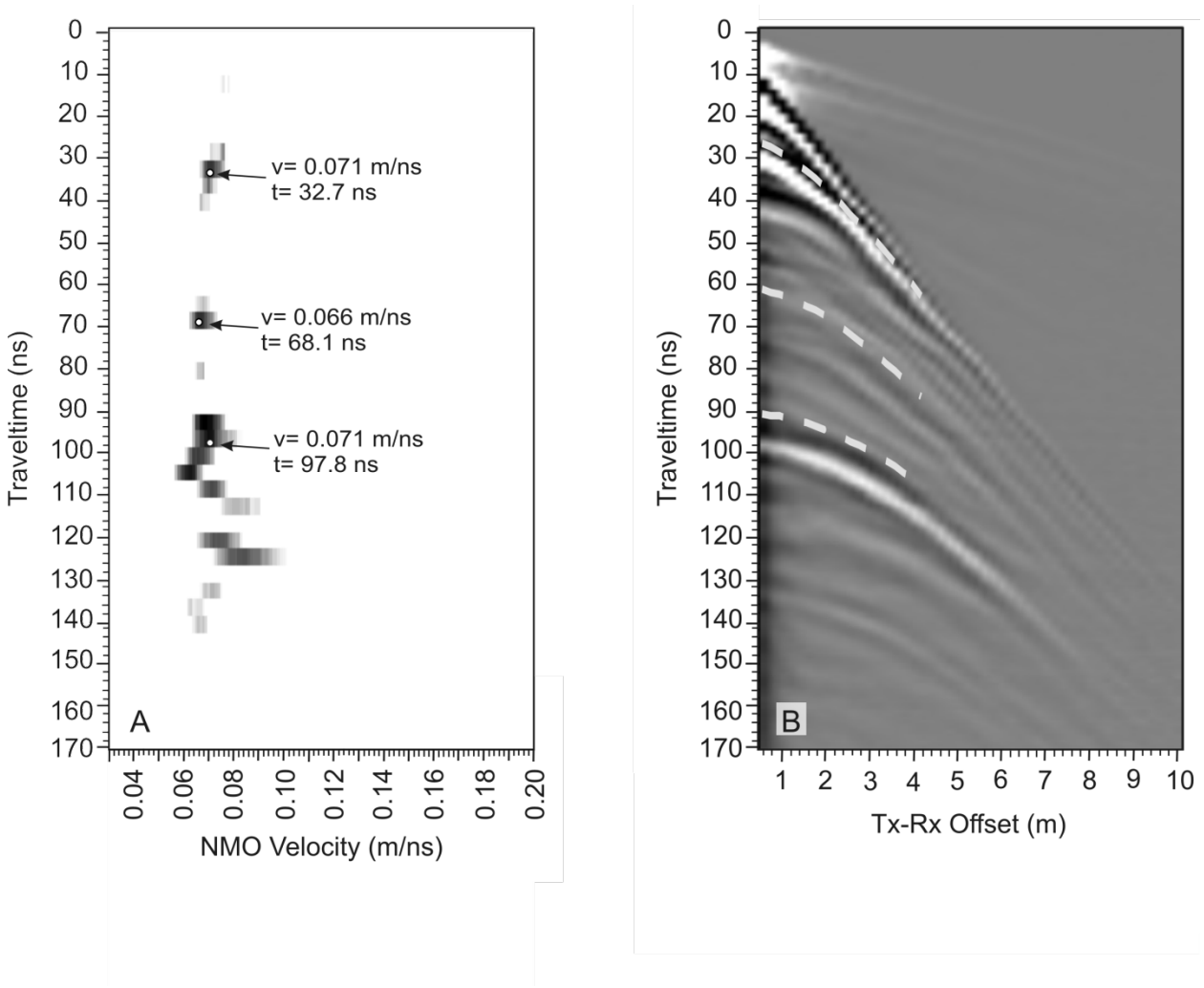


Figure 3. Semblance analysis (left panel) for the GPR CMP sounding data (right panel). A) The three identified maximums in the semblance plot indicate three reflections, the shallow and deep identified in Figure 2 and an intermediate reflection. B) The CMP sounding data with predicted traveltime arrivals for the three identified reflections are provided as white dashed lines on the CMP sounding data. Velocity analysis from each phase is provided in Table 3.

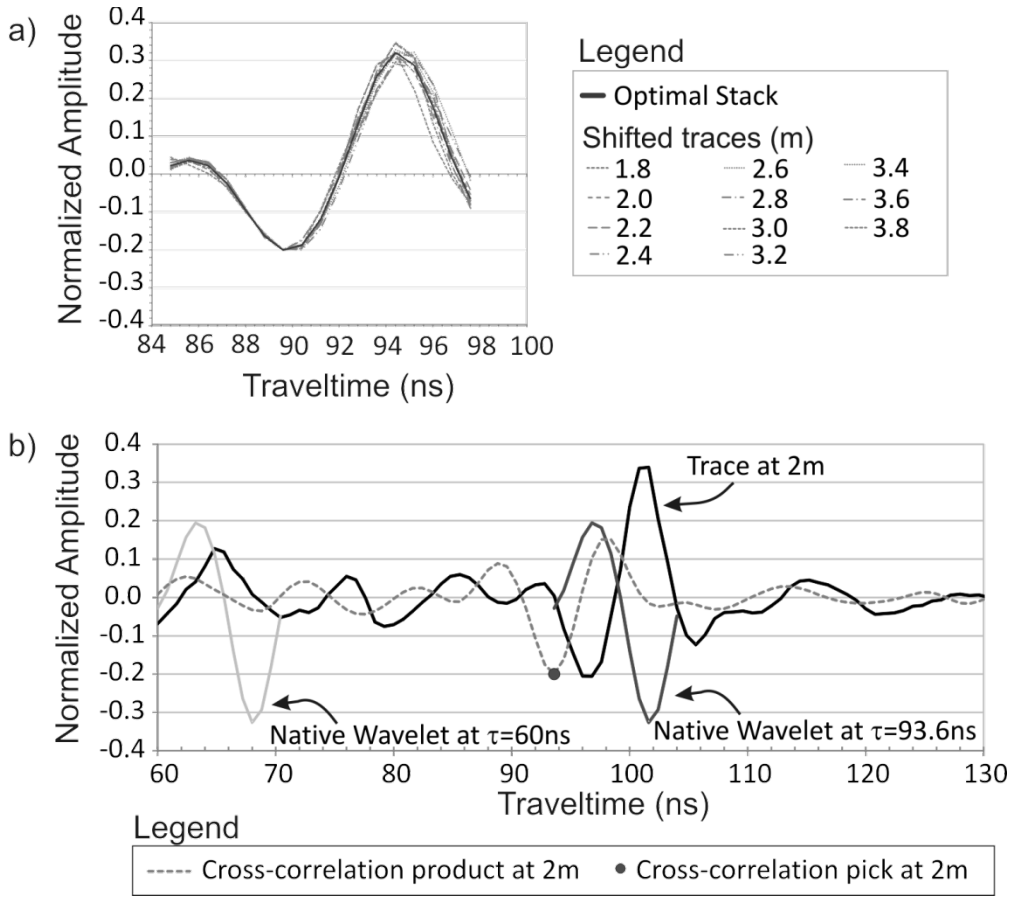


Figure 4. Cross-correlation analysis for deep reflection observed in the CMP sounding data. A) Normal moveout (NMO) corrected traces used to construct the optimal stack for the deep reflection. B) The native wavelet (based on optimal stack) is translated to larger $\tau$ (start time) and the cross-correlation product is calculated for each traveltime producing the gray-dashed line.

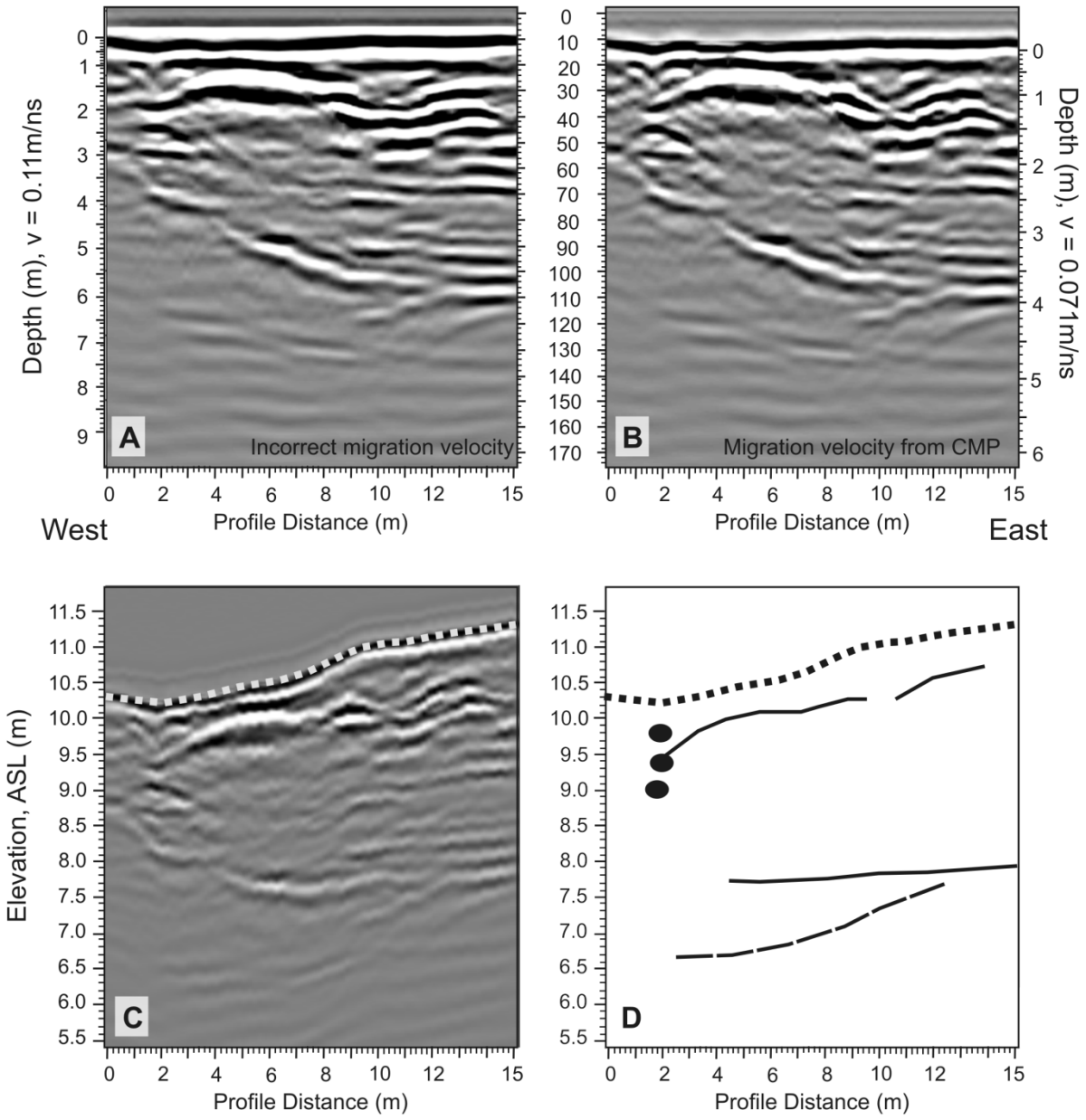


Figure 5. GPR profile corrections. In each panel, the GPR profile has been dewowed and gained with spherical spreading and attenuation correction. A) Migrated using 0.11 m/ns velocity as median velocity from diffraction analysis. B) Migrated using 0.071 m/ns velocity from CMP cross-correlation analysis on the reflection at 3.25 (±0.05) m. C) Migrated and topographically corrected using 0.071 m/ns velocity. The ground surface is shown with dotted line increasing in elevation with increasing profile distance from west to east. D) Interpreted results of GPR profile, where lines are interfaces and ovals are point scatterers. Excavation revealed the depth estimates provided from GPR survey were within the 95% confidence interval of the cross-correlation analysis.

Table 1. GPR system parameters used for both profile and CMP sounding.

| *Parameter* | *Value* |
|---|---|
| Step Size | 0.2 m |
| Stacking | 64 |
| Sample Rate | 0.8 ns |
| Time Window | 500 ns |

Table 2. Velocity analysis from point scatterers on GPR profile in Figure 1.

| Hyberpola | Position (m) | Travel-time (ns) | Velocity (m/ns) | Depth (m) |
|---|---|---|---|---|
| A | 1 | 20.5 | 0.110 | 1.1 |
| B | 1.7 | 44.5 | 0.136 | 3.0 |
| C | 4.6 | 82.1 | 0.080 | 3.3 |
| D | 9.5 | 96.1 | 0.070 | 3.4 |
| E | 12.8 | 112.1 | 0.110 | 6.2 |

Table 3. CMP sounding analysis to determine LMO velocity for Direct Air and NMO velocity of the Deep Reflection in Figure 2. Handpicks and cross-correlation for the first break of each GPR signal in Figure 2 and semblance analysis from Figure 3.

| Phase | Type of Analysis | Velocity (m/ns) | 95% C.L. (m/ns) | TWTT (ns) | 95% C.L. (ns) | Depth (m) | 95% C.L. (m) |
|---|---|---|---|---|---|---|---|
| Direct Air | Handpicks (1.2 to 4.4m) | 0.298 | 0.005 | 0 | 0.1 | | |
| | Cross-Correlation (0.6 to 4m) | 0.300 | 0.004 | 0 | 0.2 | | |
| | | | | | | | |
| Reflection Analysis | Handpicks (0.6 to 4m) | 0.069 | 0.002 | 90.4 | 0.5 | 3.1 | 0.1 |
| | Semblance (0.6 to 3.4 m) | 0.071 | 0.003 | 97.8 | 3.8 | 3.5 | 0.3 |
| | Cross-Correlation (0.6 to 4m) | 0.071 | 0.001 | 91.5 | 0.2 | 3.25 | 0.05 |

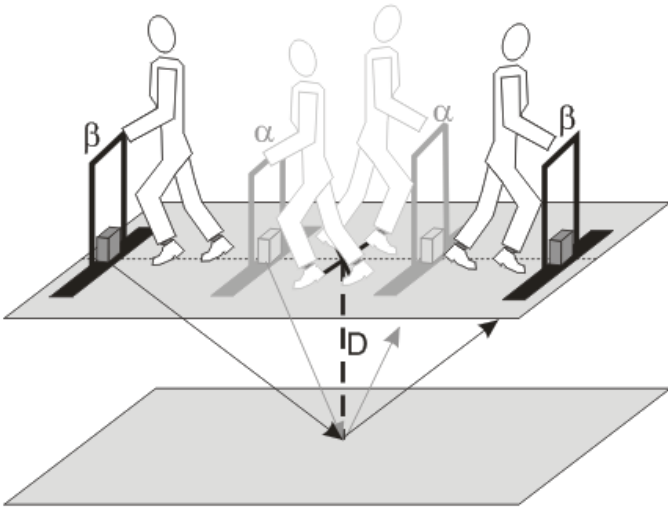


**Figure B1**. CMP sounding method. The X in middle of antenna locations represents the mid-point for the CMP sounding and two antenna positions are shown $\alpha$ and $\beta$ where the distance between the antennas is the Tx-Rx offset. The depth (D) to the subsurface reflecting interface is shown along with the raypath for the reflected signal. (after Hermance, 2001, personal communication)

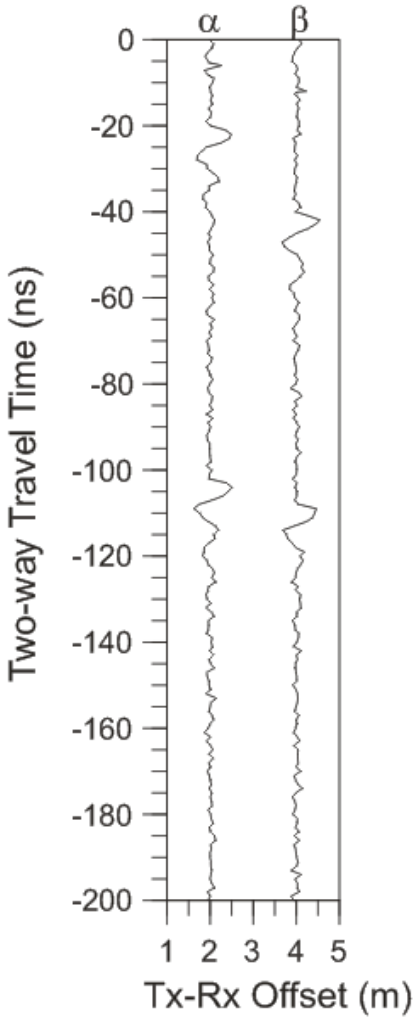


**Figure B2.** Theoretical GPR traces collected at Tx-Rx offset $\alpha$ and $\beta$ from Figure B1. GPR signals are shown for the direct air, and shallow and deeper reflections.